

# Prediction of large thermoelectric figure of merit in n-type PbTe driven near the soft-mode phase transition via lattice expansion

Jiang Cao,<sup>1,2,\*</sup> Đorđe Dangić,<sup>2,3</sup> José D. Querales-Flores,<sup>2</sup> Stephen Fahy,<sup>2,3</sup> and Ivana Savić<sup>2,†</sup>

<sup>1</sup>*School of Electronic and Optical Engineering, Nanjing University of Science and Technology, Nanjing 210094, China*

<sup>2</sup>*Tyndall National Institute, Dyke Parade, Cork T12R5CP, Ireland*

<sup>3</sup>*Department of Physics, University College Cork, College Road, Cork T12K8AF, Ireland*

(Dated: January 21, 2021)

IV-VI materials are some of the most efficient bulk thermoelectric materials due to their proximity to soft-mode phase transitions, which leads to low lattice thermal conductivity. However, the effect of soft phonon modes on their electronic thermoelectric properties remains poorly understood. Using first principles calculations, we show that the soft zone center transverse optical phonons do not deteriorate the electronic thermoelectric properties of PbTe driven closer to the phase transition via lattice expansion due to external stress. Scattering between electrons and soft phonons remains weak even very near the phase transition as a result of symmetry restrictions. In contrast, phonon softening considerably reduces the lattice thermal conductivity of PbTe with the lattice constants  $\sim 1.5\%$  larger than that at equilibrium and doubles the thermoelectric figure of merit. Our results indicate that the thermoelectric figure of merit of materials with soft phonon modes that interact strongly with other phonons, but weakly with electronic states relevant for transport, could be significantly increased by bringing these materials closer to the soft-mode phase transition.

## I. INTRODUCTION

The metric by which the performance of a thermoelectric material is measured is the thermoelectric figure of merit,  $ZT = (\sigma S^2 T)/(\kappa_e + \kappa_L)$ , where  $S$  is the Seebeck coefficient,  $\sigma$  is the electrical conductivity,  $T$  is the temperature, and  $\kappa_e$  and  $\kappa_L$  are the electronic and lattice contribution to thermal conductivity, respectively<sup>1-3</sup>. Achieving high  $ZT$  values requires a high power factor ( $PF=S^2\sigma$ ) and low  $\kappa_e$  and  $\kappa_L$ . The electronic transport properties  $S$ ,  $\sigma$  and  $\kappa_e$  are correlated, while  $\kappa_L$  is to some degree independent from the electronic properties in semiconductors.

Reducing  $\kappa_L$  without changing electronic transport properties in a material is a frequently used approach for improving  $ZT$ , known as the “phonon glass-electron crystal”<sup>4,5</sup>. It has been recently recognized that the proximity to soft-mode phase transitions is one of the key ingredients in suppressing the lattice thermal conductivity of IV-VI thermoelectric materials<sup>6-12</sup>. Bringing SnSe near its soft-mode phase transition via temperature has been shown to enhance anharmonicity and reduce  $\kappa_L$ <sup>12-15</sup>. Similar effects have also been predicted for PbTe driven to a different type of the soft-mode phase transition via strain or alloying<sup>6,16</sup>. An important open question is whether soft phonon modes can lead to strong electron-phonon (e-ph) scattering, and actually reduce the PF, thus competing with the benefit of lowering  $\kappa_L$  for improved thermoelectric performance.

We have recently shown using first principles calculations that soft phonon modes in PbTe interact weakly with the electronic states relevant for thermoelectric transport<sup>17,18</sup>. On the other hand, recent first principles calculations in SrTiO<sub>3</sub> have revealed that soft phonon modes become the dominant e-ph scattering channel near the Curie temperature<sup>19</sup>. In order to fully assess whether

structural phase transitions can be exploited for increasing thermoelectric efficiency, it is necessary to gain more insight on how e-ph scattering and electronic transport properties will change in the vicinity of the phase transitions. However, there are few if any first-principles studies of e-ph interactions in thermoelectric materials driven close to soft-mode phase transitions.

In this paper, we show from first principles calculations that driving n-type PbTe close to its soft-mode phase transition via lattice expansion due to external stress does not degrade the electronic transport properties and increases  $ZT$ . Near the phase transition, the soft transverse optical (TO) phonon mode frequencies at the zone center collapse, causing strong anharmonicity and scattering with heat-carrying acoustic phonons<sup>6,7,9</sup>. We show that this effect can reduce  $\kappa_L$  by more than a factor of 2. We find that soft TO modes interact more strongly with the electronic states determining thermoelectric transport as PbTe approaches the phase transition. However, soft TO modes remain a relatively weak e-ph scattering channel compared to long-range polar longitudinal optical (LO) phonon modes, due to symmetry restrictions. Consequently, increasing the proximity to the soft TO mode phase transition via lattice expansion does not have a detrimental effect on the electronic thermoelectric properties of PbTe and nearly doubles the maximum value of  $ZT$ .

## II. METHOD

### A. Phonons and lattice thermal conductivity

To describe the anharmonic behavior of PbTe near the soft-mode phase transition, we calculated the phonon frequencies and eigenvectors using the temperature-

dependent effective potential (TDEP) method<sup>20–22</sup>. The TDEP method extracts effective interatomic force constants (IFCs) through an efficient fitting procedure of the potential energy surface at a given temperature. For the TDEP calculations, we prepared 12 configurations of a 512 atom supercell with thermal displacements at 50 K<sup>23</sup>. The temperature of 50 K was heuristically chosen to be low while generating sufficiently large thermal displacements to achieve high accuracy of the fitting procedure. The lattice constants in these and electronic transport calculations include strain induced by external stress and neglect strain due to thermal expansion. Next we performed density functional theory (DFT) calculations on these supercells using the ABINIT package<sup>24,25</sup> and the local density approximation (LDA)<sup>26</sup> excluding spin-orbit coupling (SOC). We used the Hartwigsen-Goedecker-Hutter (HG) norm-conserving pseudopotentials<sup>27</sup> with the cutoff energy of 16 Ha. We then collected the computed forces and displacements, from which we extracted the effective second- and third-order IFCs. To obtain the converged phonon properties at 50 K, we performed an iterative procedure, where the atomic displacements used to construct the trial phonon Hamiltonian depend on the previous iteration<sup>23</sup>. Using the effective IFCs, we calculated anharmonic phonon band structures and lattice thermal conductivities by solving the phonon Boltzmann equation within the relaxation time approximation<sup>6,23</sup>.

## B. Electronic thermoelectric transport

To account for the phonon renormalization due to anharmonicity, as well as the temperature dependence of electronic band structure, we employed the thermoelectric transport model developed in our previous work and tested for PbTe against many experiments<sup>17,18,28</sup>. We calculated all the parameters of the model from first principles, thus relying on no free parameters. We accounted for the anharmonic renormalization of phonon frequencies by inserting the TDEP results into the model.

The electronic band structure was calculated using the VASP package<sup>29</sup> and the screened Heyd-Scuseria-Ernzerhof (HSE03) hybrid functional including SOC<sup>30,31</sup>. The basis set for the one-electron wave functions was constructed with the projector augmented wave method<sup>32</sup>. We performed a full structural optimization using the HSE03 hybrid functional and obtained the lattice constant of 6.517 Å. The HSE03 lowest conduction band was fitted to the two-band Kane model near the L points, using the parallel and perpendicular effective masses ( $m_{\perp,\parallel}^*$ ) and the non-parabolic parameter set to the inverse of the bandgap ( $1/E_g$ )<sup>17</sup>.

In our electronic transport model, we also accounted for the temperature dependence of the bandgap due to e-ph interactions. We calculated  $\partial E_g/\partial T = 2.98 \times 10^{-4}$  eV/K<sup>33</sup> using the non-adiabatic Allen-Heine-Cardona formalism<sup>34–36</sup> and density functional perturba-

tion theory (DFPT)<sup>37,38</sup>, as implemented in ABINIT<sup>39</sup>. The effective masses are taken to depend on temperature as  $m_{\perp,\parallel}^*(T)/m_{\perp,\parallel}^*(0\text{K}) = E_g(T)/E_g(0\text{K})$  according to the two-band Kane model<sup>40</sup>. We note that the thermal expansion contribution to  $\partial E_g/\partial T$  is excluded in this study since we explicitly investigate the effect of lattice expansion on thermoelectric transport.

To calculate e-ph relaxation times, we first computed e-ph matrix elements within the DFPT framework as implemented in the QUANTUM ESPRESSO package<sup>41,42</sup>, using the LDA excluding SOC with the HG norm-conserving pseudopotentials. In our previous work, we verified that the LDA without SOC gives very similar e-ph matrix elements compared with the HSE03 with SOC<sup>43</sup>. For the LDA with SOC, the e-ph matrix elements are ill-defined, because the conduction band minimum and valence band maximum states are interchanged and mix heavily, forming an incorrect "negative bandgap"<sup>43</sup>. In our DFPT calculations of e-ph matrix elements, we used  $12 \times 12 \times 12$  and  $6 \times 6 \times 6$  reciprocal space grids for electronic and phonon states, respectively, and the cutoff energy was set to 70 Ry. E-ph matrix elements were then interpolated on finer  $40 \times 40 \times 40$   $\mathbf{k}$  and  $\mathbf{q}$ -grids using the Wannier functions method and the EPW code<sup>44</sup>. Fourteen Wannier orbitals were constructed from Bloch states on a  $12 \times 12 \times 12$   $\mathbf{k}$ -point grid using the Wannier90 code<sup>45</sup>.

We note that our computed e-ph matrix elements do not account for the anharmonic renormalization of phonon eigenvectors, as done in Ref. 19. We checked this assumption by analyzing the projections of the anharmonic eigenvectors obtained from TDEP onto the harmonic eigenvectors for PbTe with and without lattice expansion. We found that they do not differ considerably for phonons near the zone centre in all cases, which are the only contributors to electronic transport in PbTe<sup>17</sup>. Furthermore, our previous calculations of the electronic thermoelectric properties of PbTe without lattice expansion using the harmonic eigenvectors are in excellent agreement with experiments<sup>17,18,28</sup>.

We parametrized nonpolar and polar Fröhlich e-ph scattering mechanisms using the approach developed in our previous work<sup>17,43</sup>. Acoustic and optical deformation potentials were calculated by fitting the corresponding e-ph matrix elements with the deformation potential Hamiltonian in the long-wavelength limit along five high-symmetry directions of  $\mathbf{q}$  in a cubic crystal<sup>43,46,47</sup>. Ionized-impurity scattering induced by the dopant atoms was accounted for using the Brooks-Herring model<sup>48</sup> with the Thomas-Fermi screening. Elastic and dielectric constants for the polar Fröhlich perturbation Hamiltonian were obtained from DFPT.

Electronic transport quantities were calculated using the Boltzmann transport theory within the transport

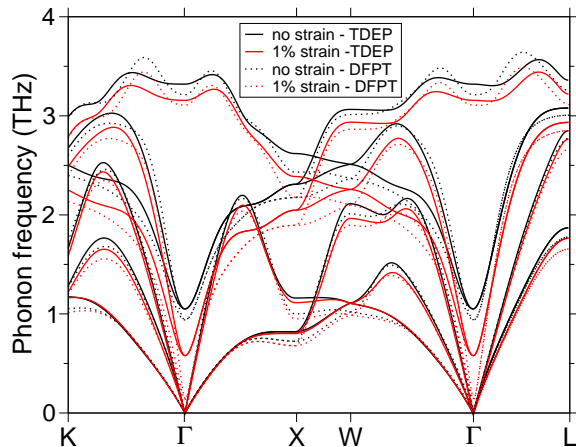


FIG. 1. Phonon dispersion for PbTe with the equilibrium lattice constant (black lines) and the 1% larger lattice constant (red lines). Solid lines represent the results computed using the temperature dependent effective potentials (TDEP) method at 50 K, while dotted lines are obtained using density functional perturbation theory (DFPT).

(momentum) relaxation time approximation as

$$\begin{cases} \sigma &= L_0, \\ S &= -L_1/(eTL_0), \\ \kappa_0 &= L_2/(e^2T), \end{cases} \quad (1)$$

where  $\sigma$  is the electrical conductivity tensor,  $S$  is the Seebeck coefficient tensor,  $\kappa_0$  is the thermal conductivity tensor defined when the electric field across the material is zero, and  $e$  is the electron charge value. The transport kernel functions for the conduction band are defined by

$$L_\alpha = \int_{\text{BZ}} \frac{e^2 d\mathbf{k}}{4\pi^3} \left( -\frac{\partial f}{\partial E} \right) \tau_{\mathbf{k},\text{tot}} \bar{v}_{\mathbf{k}}^2 (E_{\mathbf{k}} - E_F)^\alpha, \quad (2)$$

where  $E_{\mathbf{k}}$  is the energy of the conduction band state with the crystal momentum  $\mathbf{k}$ ,  $\bar{v}_{\mathbf{k}} = [\sum_i (v_{\mathbf{k}}^i)^2/3]^{1/2}$  is the group velocity averaged over directions,  $i$  denotes the Cartesian directions,  $f$  is the Fermi-Dirac distribution function,  $E_F$  is the Fermi level, and  $\tau_{\mathbf{k},\text{tot}}$  is the total transport relaxation time of all scattering channels<sup>17</sup>.

### III. RESULTS AND DISCUSSION

#### A. Transverse optical mode softening

PbTe crystallizes in the rocksalt structure up to the melting temperature of  $\sim 1200$  K<sup>49</sup>. Nevertheless, it is energetically close to the phase transition to the rhombohedral phase, characterized by the internal atomic displacement of Te, which corresponds to a frozen-in atomic motion of the zone center TO mode along the [111] direction in the rocksalt structure. As a result, the TO phonon modes near the zone center in PbTe are very

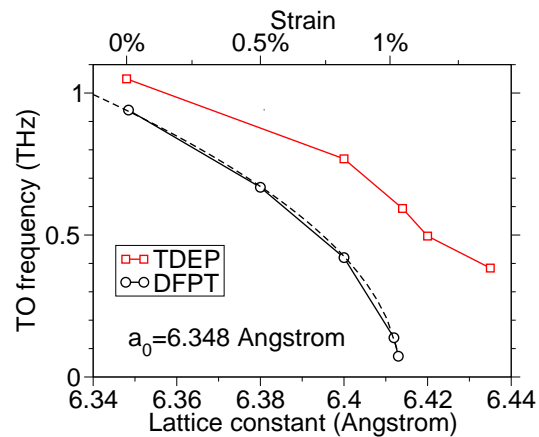


FIG. 2. Frequency of transverse optical (TO) modes at the zone center for PbTe versus lattice constant and strain, calculated using density functional perturbation theory (DFPT, black circles) and the temperature-dependent effective potential (TDEP) method at 50 K (red squares). The dashed black line represents a fit to the DFPT results.

soft<sup>8,50</sup>, see the black solid lines in Fig. 1. If the lattice is expanded via external stress, the frequencies of the soft TO modes near the  $\Gamma$  point further decrease (red solid lines in Fig. 1), since the potential energy surface flattens as PbTe approaches the soft-mode phase transition.

In Fig. 1, we compare the harmonic phonon dispersion obtained using DFPT and the renormalized phonon dispersion from the TDEP at 50 K method for PbTe with the equilibrium lattice constant and the lattice constant expanded by 1%. In the TDEP calculation, the interatomic force constants to all orders are implicitly accounted for through searching for the best possible fit of the potential energy surface, while DFPT does not include the terms higher than the second order. For PbTe with the equilibrium lattice constant, the TDEP phonon dispersion of PbTe is very similar to the DFPT result. This is because PbTe is still relatively far from the soft-mode phase transition, and higher order anharmonic terms are not prominent. For PbTe with the increased lattice constant, the TDEP calculation gives harder TO modes than DFPT, since anharmonicity substantially increases closer to the phase transition. For the LO and acoustic modes of PbTe under 1% of strain, the TDEP and DFPT calculations give very similar results that are much less sensitive to changes of the lattice constant compared to the soft TO modes.

To gain more insight into the TO mode behavior near the soft-mode phase transition, Fig. 2 shows the soft TO mode frequency at the  $\Gamma$  point,  $\omega_{\text{TO}}^\Gamma$ , as a function of the lattice constant and the corresponding strain. The  $\omega_{\text{TO}}^\Gamma$  computed from DFPT can be fitted to  $\omega_{\text{TO}}^\Gamma = \alpha \sqrt{a_c - a_{\text{latt}}}$ , with  $\alpha = 3.67246$  THz  $\text{\AA}^{-0.5}$  and  $a_c = 6.41338$   $\text{\AA}$ , shown by the black dashed line in Fig. 2. The TDEP method at 50 K gives harder  $\omega_{\text{TO}}^\Gamma$  than DFPT, which does not reach zero at the phase transition,

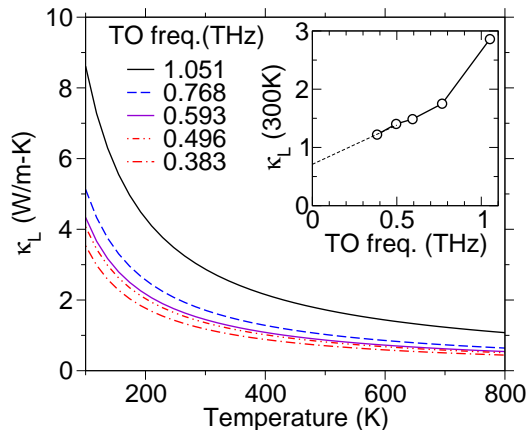


FIG. 3. Lattice thermal conductivity ( $\kappa_L$ ) versus temperature for different values of the frequency of soft transverse (TO) modes at the zone center ( $\omega_{\text{TO}}^{\Gamma}$ ), obtained using the temperature dependent effective potentials (TDEP) method using the interatomic force constants at 50 K. The inset shows  $\kappa_L$  at 300 K as a function of  $\omega_{\text{TO}}^{\Gamma}$ . The dashed line in the inset represents the linear extrapolation of the  $\kappa_L$  values down to zero  $\omega_{\text{TO}}^{\Gamma}$ .

even though it decreases with increasing strain. When the material becomes strongly anharmonic close to the phase transition, the harmonic phonon dispersion from DFPT is not sufficient for describing the vibrational and thermal properties, and including anharmonic terms as implemented in the TDEP method becomes crucial.

### B. Lattice thermal conductivity

Next we investigate the impact of lattice expansion and TO mode softening on the lattice thermal conductivity of PbTe. Figure 3 reports the temperature dependence of  $\kappa_L$  for different values of  $\omega_{\text{TO}}^{\Gamma}$  obtained using the TDEP method, which correspond to different values of strain indicated in Fig. 2. We note that the interatomic force constants (IFCs) are functions of temperature, while we only use the IFCs at 50 K in this study. We will discuss in Sec. III F that this is a valid approximation in PbTe without introducing qualitative changes to the results in this work. In our calculations,  $\kappa_L$  decreases inversely proportional to temperature for all considered values of  $\omega_{\text{TO}}^{\Gamma}$  and strain, due to changes in phonon populations.  $\kappa_L$  at 300 K (and all other temperatures) decreases substantially as  $\omega_{\text{TO}}^{\Gamma}$  decreases (see the inset of Fig. 3). The linear extrapolation of the  $\kappa_L$  values at 300 K when  $\omega_{\text{TO}}^{\Gamma}$  reaches 0 THz is around  $0.75 \text{ Wm}^{-1}\text{K}^{-1}$ , which is less than 1/3 of the value for the equilibrium structure. As PbTe approaches the phase transition and the TO modes become softer, anharmonicity becomes substantially stronger with respect to the equilibrium structure and contributes to the  $\kappa_L$  decrease. In addition, the frequencies of soft TO modes and heat-carrying acoustic

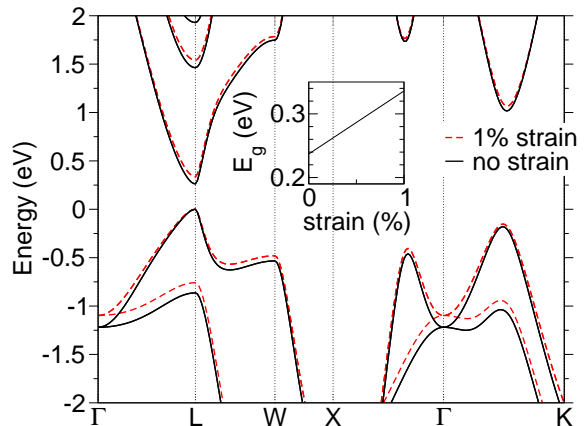


FIG. 4. Electronic band structure at 0 K for PbTe with the equilibrium lattice constant (solid black lines) and the 1% larger lattice constant (dashed red lines). The inset shows direct bandgap versus strain.

modes become more similar closer to the phase transition (Fig. 1), thus increasing the scattering phase space and further reducing  $\kappa_L$ . We also note that the  $\kappa_L$  calculated using DFPT would be even lower than that using the TDEP method for the same lattice constant, due to the much softer TO modes obtained with DFPT.

### C. Electronic band structure

PbTe has the conduction band minima (CBM) and the valence band maxima (VBM) located at the four L points in the BZ. In Fig. 4, we plot the electronic band structure calculated using the HSE03 hybrid functional for PbTe with the equilibrium and expanded lattice constants ( $a_{\text{latt}} = a_0$  and  $a_{\text{latt}} = 1.01a_0$ , respectively.) Most importantly, strain has a fairly weak effect on the electronic band structure close to the Fermi energy. The direct bandgap at the L points ( $E_g$ ) is increased from 0.238 eV to 0.336 eV by applying 1% of strain, as shown in the inset of Fig. 4. The conduction and valence band effective masses increase with the bandgap. We can accurately fit the HSE03 conduction band within 0.5 eV from the CBM using the Kane model if we use  $1/E_g$  as the non-parabolic parameter of the Kane model, and the effective masses calculated using the LDA without SOC given in Table I.

### D. Electron-phonon interaction

To accurately describe the e-ph interaction in n-type PbTe driven close to the phase transition via lattice expansion, all the relevant quantities<sup>17</sup> were calculated from first principles for the equilibrium and 1% expanded lattice constants, as reported in Table I. The acoustic and

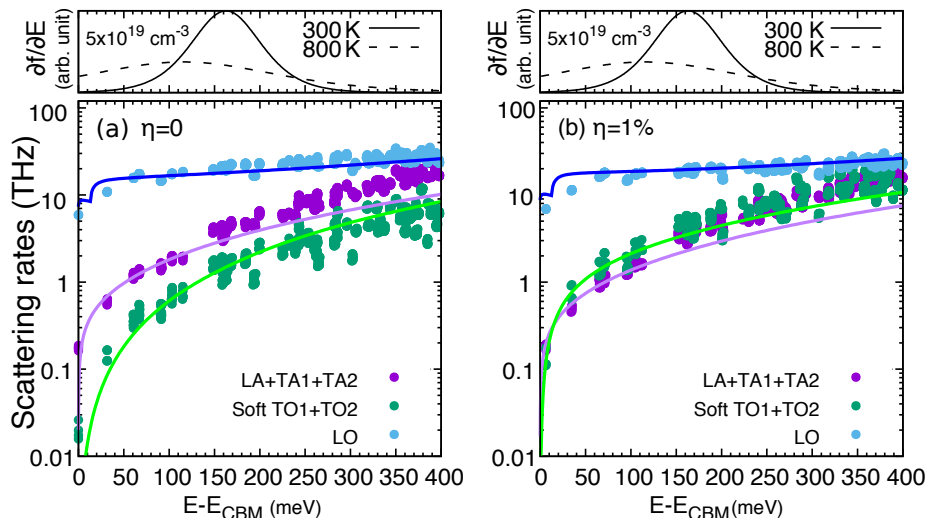


FIG. 5. Electron-phonon scattering rates at 300 K resolved by phonon mode as a function of electronic energy for PbTe with (a) no applied strain ( $\eta=0$ ) and (b) 1% of strain ( $\eta=1\%$ ). The energy derivative of the Fermi distribution function for the doping concentration of  $5 \times 10^{19} \text{ cm}^{-3}$  is also plotted for 300 K and 800 K. The zero of the energy axis is the conduction band minimum.

$\eta$	0	1%
$a_{\text{latt}}$ (Å)	6.348	6.411
$\Xi_d^{\text{ac}}$ (eV)	0.37	0.36
$\Xi_u^{\text{ac}}$ (eV)	7.03	6.48
$\Xi_d^{\text{opt}}$ (eV)	19.09	19.56
$\Xi_u^{\text{opt}}$ (eV)	-34.24	-34.79
$\omega_{\Gamma}^{\text{LO}}$ (THz)	3.2	3.1
$\omega_{\Gamma}^{\text{TO}}$ (THz)	0.95	0.15
$\epsilon_{\infty}$	34.85	33.59
$\epsilon_s$	356.8	14346
$c_{11}$ (GPa)	136.4	120.6
$c_{12}$ (GPa)	3.8	4.5
$c_{44}$ (GPa)	17.1	17.0
$E_g^{\text{HSE}}$ (eV)	0.238	0.336
$m_{\parallel}^*/m_0$	0.216	0.241
$m_{\perp}^*/m_0$	0.037	0.043

TABLE I. Parameters used in the calculation of electronic transport quantities and computed from first principles for n-type PbTe with the equilibrium lattice constant (no strain,  $\eta = 0$ ) and the lattice constant expanded by 1% ( $\eta = 1\%$  of strain): lattice constant in the local density approximation ( $a_{\text{latt}}$ ), acoustic deformation potentials ( $\Xi_d^{\text{ac}}$  and  $\Xi_u^{\text{ac}}$ ), optical deformation potentials ( $\Xi_d^{\text{opt}}$  and  $\Xi_u^{\text{opt}}$ ), optical phonon frequencies ( $\omega_{\Gamma}^{\text{LO}}$  and  $\omega_{\Gamma}^{\text{TO}}$ ), high-frequency and static dielectric constants ( $\epsilon_{\infty}$  and  $\epsilon_s$ ), elastic constants ( $c_{11}$ ,  $c_{12}$  and  $c_{44}$ ), direct bandgap from the hybrid functional calculations ( $E_g^{\text{HSE}}$ ), and parallel and perpendicular effective masses at the conduction band minimum ( $m_{\parallel}^*$  and  $m_{\perp}^*$ ).

optical deformation potentials and the high-frequency dielectric constant  $\epsilon_{\infty}$  do not change much with strain because the electronic band structure of PbTe is relatively insensitive to strain (Fig. 4). Similarly, the elastic con-

stants do not vary considerably with strain, reflecting the same trend seen for acoustic phonon branches, as well as the LO phonon frequency (Fig. 1). The only quantities that change significantly while varying the amount of strain are the TO phonon frequency  $\omega_{\text{TO}}^{\Gamma}$  (Fig. 1) and the static dielectric constant  $\epsilon_s$ . For this reason, in the following calculations, we will only update the values of  $\omega_{\text{TO}}^{\Gamma}$  and  $\epsilon_s$  as a function of strain, as well as the parameters of the electronic band structure i.e. the bandgap and the effective masses.

Next we compute the e-ph scattering rates of PbTe using our model, and compare them with those obtained using the EPW code, which makes no assumptions about the  $\mathbf{k}$ - and  $\mathbf{q}$ -point dependence of e-ph matrix elements and their changes with strain<sup>44</sup>. In the EPW calculations, we used  $40 \times 40 \times 40$   $\mathbf{k}$ - and  $\mathbf{q}$ -point grids, and the Gaussian broadening parameter was set to 40 meV. Figure 5 shows the mode-resolved e-ph scattering rates for n-type PbTe under different strain conditions at 300 K, calculated using our model and the EPW code. We note that the model is in very good agreement with the EPW results for all the phonon modes and for different strain values. This finding highlights the accuracy of our model and further justifies our assumption of keeping the acoustic and optical deformation potentials,  $\epsilon_{\infty}$  and the elastic constants constant.

Scattering due to LO phonons is the strongest e-ph scattering mechanism in equilibrium PbTe, while scattering due to soft TO phonons is the weakest [Fig. 5 (a)]. The latter effect arises because the electron-TO mode matrix element is zero by symmetry for the conduction (and valence) band states at L and the zone center TO modes in the rocksalt structure<sup>17</sup>. Since the center of inversion in PbTe is the Pb or Te site, all  $\Gamma$  and X point

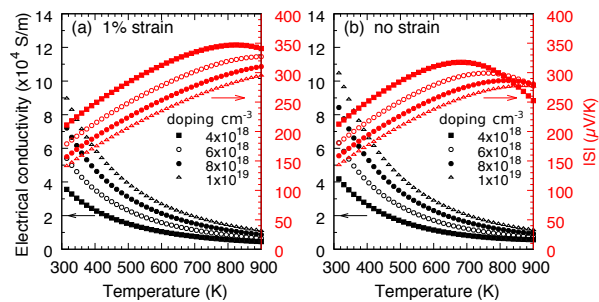


FIG. 6. Electrical conductivity and absolute Seebeck coefficient ( $|S|$ ) as a function of temperature for PbTe: (a) with 1% strain and (b) without strain, for the doping concentrations of  $4 \times 10^{18}$ ,  $6 \times 10^{18}$ ,  $8 \times 10^{18}$  and  $1 \times 10^{19}$   $\text{cm}^{-3}$ .

phonons have odd parity under inversion symmetry<sup>51</sup>. Odd parity phonons couple only electronic states of opposite parity since e-ph matrix elements are invariant under symmetry operations<sup>51</sup>. The e-ph matrix-elements containing the  $\Gamma$  point phonons thus vanish exactly at the L points in PbTe since the initial and final electronic states are of the same parity. Similarly, the intervalley L-L scattering caused by the X-point phonons also vanishes.

Nevertheless, the strength of electron-TO phonon scattering increases as PbTe approaches the phase transition due to lattice expansion, as shown in Fig. 5. One of the reasons for that is that soft TO modes become softer and the phonon population and the vibration amplitude corresponding to TO modes increase. In addition, lowering the TO mode frequency near the zone center means that the energy and momentum conservation conditions for scattering become easier to satisfy, hence increasing the electron-TO phonon scattering phase space. In comparison, polar LO phonon scattering and acoustic phonon scattering are much less sensitive to strain. Within the energy range relevant for electronic transport properties, polar LO phonon scattering is still stronger than that of acoustic and TO phonons even for 1% strain. Due to this predominant role of polar LO phonon scattering, strain has a much weaker influence on the total e-ph scattering in PbTe compared to phonon-phonon scattering.

### E. Electronic thermoelectric properties and $ZT$

To elucidate the effect of the soft-mode phase transition on electronic transport in PbTe, we illustrate the temperature dependence of the electrical conductivity and the Seebeck coefficient at different doping levels for PbTe with no strain and 1% of strain in Fig. 6. Increasing the lattice constant results in a wider electronic bandgap (Fig. 4). This reduces the minority carrier concentration and the bipolar effect that causes a drop of the Seebeck coefficient at high temperatures and low doping concentrations<sup>28</sup>. Therefore, strain leads to an improvement of the Seebeck coefficient above 600 K. A larger bandgap due to strain also flattens the conduction band

and leads to larger effective masses at the band edge, which explains the higher peak value of the Seebeck coefficient closer to the phase transition. On the other hand, due to larger effective masses, the electrical conductivity is inevitably reduced with lattice expansion. We note that the electronic band structure changes as a result of strain have a stronger effect on the electronic transport properties than the changes in the scattering rates. This is because the dominant LO phonon scattering rate does not change much when PbTe is driven closer to the phase transition via lattice expansion. In addition, we note that the contribution of ionized impurity scattering to the electron scattering rates is much smaller than that of phonons at room temperature and above in PbTe with no strain<sup>17</sup>. When the TO modes soften, the static dielectric constant increases (see Table I), thus leading to a reduction in the ionized impurity scattering and a negligible effect on the electron scattering rates.

To further understand the role played by the closeness to the phase transition on the thermoelectric transport properties of PbTe, in Fig. 7 we plot all the relevant properties as a function of the doping concentration for different values of  $\omega_{\text{TO}}^{\Gamma}$  obtained from the TDEP calculations (see Fig. 2). The electrical conductivity is not influenced by the proximity to the phase transition for the doping concentrations lower than  $1 \times 10^{20}$   $\text{cm}^{-3}$ , even though the TO phonon scattering increases in magnitude. The absolute value of the Seebeck coefficient practically does not change with  $\omega_{\text{TO}}^{\Gamma}$ . The total thermal conductivity decreases significantly with  $\omega_{\text{TO}}^{\Gamma}$  for all doping concentrations. The major part of the  $\kappa$  reduction due to the increased proximity to the phase transition comes from the decrease in  $\kappa_L$ , shown in Fig. 3. The thermoelectric power factor decreases slightly in the peak value closer to the phase transition, since the electrical conductivity is lower compared to equilibrium. Therefore, driving PbTe closer to the phase transition via lattice expansion does not appreciably degrade the electronic thermoelectric properties.

Next we explore how the thermoelectric figure of merit  $ZT$  of n-type PbTe depends on the value of  $\omega_{\text{TO}}^{\Gamma}$ . We report in Fig. 8(a) the  $ZT$  values at 300 K as a function of the doping concentration for different values of  $\omega_{\text{TO}}^{\Gamma}$ . As PbTe approaches the phase transition via applied strain and  $\omega_{\text{TO}}^{\Gamma}$  decreases,  $ZT$  is increased over all doping concentrations. The optimum doping concentration slightly decreases from  $\sim 3 \times 10^{18}$   $\text{cm}^{-3}$  to  $\sim 2 \times 10^{18}$   $\text{cm}^{-3}$ , due to an increase in the effective masses. The increased proximity to the soft-mode phase transition not only decreases the total thermal conductivity but also keeps the power factor almost intact as observed in Fig. 7, which is the main factor for the increase in the  $ZT$  values.

Figure 8(b) shows the maximum  $ZT$  obtained at the optimum doping concentration as a function of  $\omega_{\text{TO}}^{\Gamma}$  at 300 K and 600 K. An increase of  $ZT_{\text{max}}$  can be achieved both at low and high temperatures by driving PbTe to the verge of the soft-mode phase transition. The reason for this is that the soft TO phonon mode that

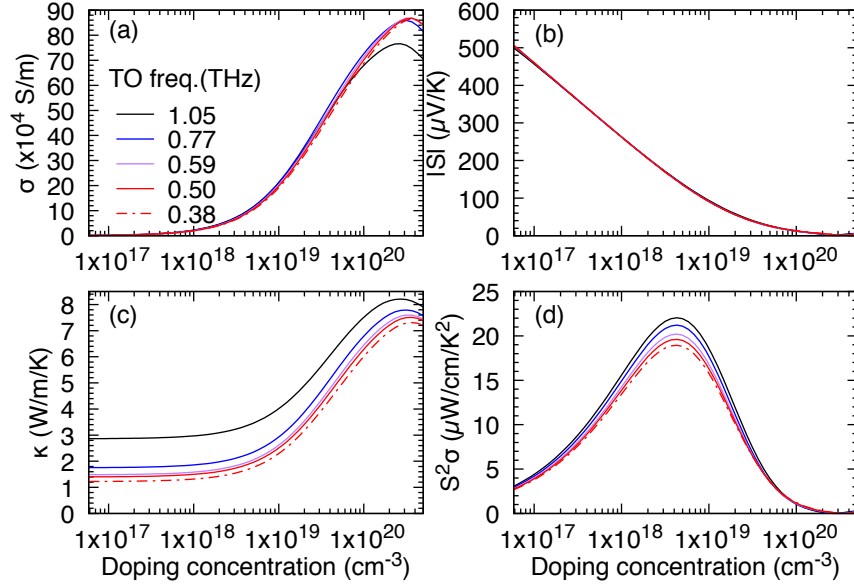


FIG. 7. Thermoelectric transport properties as a function of doping concentration at 300 K for different transverse optical (TO) phonon frequencies at the zone center obtained by applying strain: (a) electrical conductivity ( $\sigma$ ), (b) Seebeck coefficient ( $|S|$ ), (c) total thermal conductivity ( $\kappa$ ) and (d) power factor ( $\sigma S^2$ ).

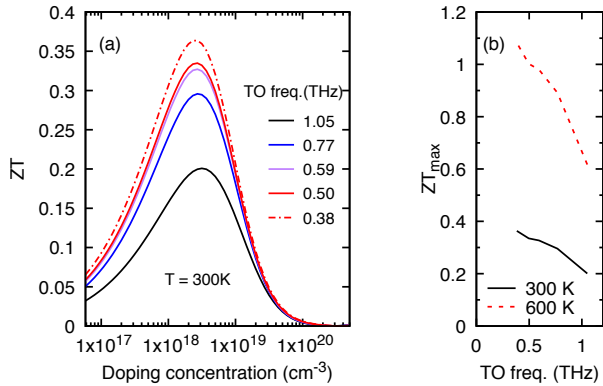


FIG. 8. (a) Thermoelectric figure of merit ( $ZT$ ) as a function of doping concentration at 300 K. (b) Maximum figure of merit ( $ZT_{\max}$ ), calculated by optimizing the doping concentration, as a function of the transverse optical (TO) phonon frequency at the zone center for 300 K and 600 K.

promotes the instability towards the phase transition is not the dominant e-ph scattering channel. On the other hand, polar LO phonon scattering is the strongest scattering mechanism and is fairly constant towards the phase transition. This specific feature of the e-ph interaction in PbTe allows the soft-mode phase transition to effectively increase scattering of heat-carrying acoustic phonons while preserving the electronic thermoelectric properties, hence materializing the "phonon glass-electron crystal" idea without nanostructuring or alloying.

## F. Discussion

Here we discuss the approximations we made in the present study and our justifications for them. The first approximation is omitting the TO mode frequency variation with temperature in all transport calculations. Our TDEP calculations include anharmonicity at 50 K. The changes in the phonon dispersion originating from thermal expansion and increased anharmonicity at higher temperatures are not accounted for in this study. Thermal expansion, which is also a type of strain, reduces the TO phonon frequency of PbTe, while thermal fluctuations increase anharmonicity and harden the TO modes. These two opposite effects mostly counterbalance each other and result in a weak temperature dependence of the TO phonon frequency<sup>7,52</sup>. Furthermore, even though increasing temperature slightly hardens the TO mode and pushes PbTe away from the phase transition, an increased amount of strain via external stress (*e.g.* negative pressure) would compensate for this temperature effect. Since all electronic transport properties depend fairly weakly on pressure, a similar increase of  $ZT$  to that predicted here could be achieved for larger values of negative pressure. Therefore, we expect that the TO mode frequency of PbTe does not change much with temperature, and even if it does, it could be regulated by applying more negative pressure.

The second approximation is that the e-ph interaction in our study is treated using the Born-Oppenheimer and harmonic approximations (even if phonon frequencies were fully renormalized by temperature). A recent model study of Chudzinski<sup>53</sup> shows that going beyond

those approximations may be important in determining thermoelectric transport at the quantum critical phase transition for temperatures substantially lower than the Debye temperature, which is  $\sim 200$  K for PbTe. In our study, we remain relatively far from the phase transition (the lowest TO frequency considered is 0.38 THz) and focus on temperatures above 300 K. Therefore, the breakdown of the Born-Oppenheimer dynamics and the inclusion of anharmonic e-ph interaction is unlikely to qualitatively alter our conclusion for PbTe in the considered operation conditions.

Finally, we note that it would be challenging to achieve the required amount of lattice expansion necessary for a significant  $ZT$  increase ( $\sim 1.5\%$ ) by mechanical or chemical means in PbTe. However, our conclusions should not be limited only to PbTe under lattice expansion induced by external stress. We can expect a  $ZT$  increase in any material driven closer to the same type of the soft-mode phase transition whose soft TO modes weakly couple with the electronic states contributing to transport. The examples of such materials are SnTe and GeTe, which can be driven near the soft-mode phase transition via temperature.

#### IV. CONCLUSION

We computationally demonstrate a new strategy to increase the thermoelectric performance of PbTe by driving the material closer to its intrinsic soft-mode phase transition, here simulated via lattice expansion due to external stress. Using first principles calculations, we show that the zone center transverse optical phonon modes substantially soften near the phase transition, while longitu-

dinal optical and acoustic phonon modes are almost unchanged. Soft modes increase lattice anharmonicity and scattering with heat-carrying acoustic phonons, which reduces the lattice thermal conductivity by more than a half due to applied strain. Regarding electron-phonon interaction, we find that even though soft modes interact more strongly with electrons when PbTe approaches the phase transition, soft mode scattering remains relatively weak compared to longitudinal optical mode scattering. The dominant electron-longitudinal optical phonon interaction and the electronic thermoelectric properties are fairly insensitive to the proximity to the phase transition. As a result, the thermoelectric figure of merit  $ZT$  in n-type PbTe can be nearly doubled simply by increasing the proximity to the soft-mode phase transition via lattice expansion. A few well-known high-performance thermoelectric materials, such as GeTe and SnTe, undergo the same type of the soft-mode phase transition with temperature. The strategy proposed in this work suggests new opportunities to further improve the  $ZT$  values of these materials.

#### ACKNOWLEDGEMENT

We thank Olle Hellman for kindly providing us the code that implements the TDEP method. This work is supported by Science Foundation Ireland under grant numbers 15/IA/3160 and 13/RC/2077 (the later grant is cofunded under the European Regional Development Fund), and Natural Science Foundation of Jiangsu Province under grant number BK20180456. We also acknowledge the Irish Centre for High-End Computing (ICHEC) for the provision of computational facilities.

---

\* jiang.cao@njust.edu.cn

† ivana.savic@tyndall.ie

<sup>1</sup> G. J. Snyder and E. S. Toberer, *Nat. Mater.* **7**, 105 (2008).

<sup>2</sup> J. He and T. M. Tritt, *Science* **357**, 6358 (2017).

<sup>3</sup> X. Zhou, Y. Yan, X. Lu, H. Zhu, X. Han, G. Chen, and Z. Ren, *Mater. Today* **21**, 974 (2018).

<sup>4</sup> M. Beekman, D. T. Morelli, and G. S. Nolas, *Nat. Mater.* **14**, 1182 (2015).

<sup>5</sup> T. Takabatake, K. Suekuni, T. Nakayama, and E. Kaneshita, *Rev. Mod. Phys.* **86**, 669 (2014).

<sup>6</sup> R. M. Murphy, É. D. Murray, S. Fahy, and I. Savić, *Phys. Rev. B* **93**, 104304 (2016).

<sup>7</sup> A. H. Romero, E. K. U. Gross, M. J. Verstraete, and O. Hellman, *Phys. Rev. B* **91**, 214310 (2015).

<sup>8</sup> O. Delaire, J. Ma, K. Marty, A. F. May, M. A. McGuire, M.-H. Du, D. J. Singh, A. Podlesnyak, G. Ehlers, M. D. Lumsden, and B. C. Sales, *Nat. Mater.* **10**, 614 (2011).

<sup>9</sup> T. Shiga, J. Shiomi, J. Ma, O. Delaire, T. Radzyski, A. Lusakowski, K. Esfarjani, and G. Chen, *Phys. Rev. B* **85**, 155203 (2012).

<sup>10</sup> C. W. Li, O. Hellman, J. Ma, A. F. May, H. B. Cao, X. Chen, A. D. Christianson, G. Ehlers, D. J. Singh, B. C.

Sales, and O. Delaire, *Phys. Rev. Lett.* **112**, 175501 (2014).

<sup>11</sup> C. W. Li, J. Hong, A. F. May, D. Bansal, S. Chi, T. Hong, G. Ehlers, and O. Delaire, *Nat. Phys.* **11**, 1063 (2015).

<sup>12</sup> L.-D. Zhao, S.-H. Lo, Y. Zhang, H. Sun, G. Tan, C. Uher, C. Wolverton, V. P. Dravid, and M. G. Kanatzidis, *Nature* **508**, 373 (2014).

<sup>13</sup> U. Aseginolaza, R. Bianco, L. Monacelli, L. Paulatto, M. Calandra, F. Mauri, A. Bergara, and I. Errea, *Phys. Rev. Lett.* **122**, 075901 (2019).

<sup>14</sup> C. Chang, D. Wang, D. He, W. He, F. Zhu, G. Wang, J. He, and L.-D. Zhao, *Adv. Energy Mater.* **9**, 1901334 (2019).

<sup>15</sup> J. Hong and O. Delaire, *Mater. Today Phys.* **10**, 100093 (2019).

<sup>16</sup> R. M. Murphy, É. D. Murray, S. Fahy, and I. Savić, *Phys. Rev. B* **95**, 144302 (2017).

<sup>17</sup> J. Cao, J. D. Querales-Flores, A. R. Murphy, S. Fahy, and I. Savić, *Phys. Rev. B* **98**, 205202 (2018).

<sup>18</sup> R. D'Souza, J. Cao, J. D. Querales-Flores, S. Fahy, and I. Savić, *Phys. Rev. B* **102**, 115204 (2020).

<sup>19</sup> J.-J. Zhou, O. Hellman, and M. Bernardi, *Phys. Rev. Lett.* **121**, 226603 (2018).

- <sup>20</sup> O. Hellman, I. A. Abrikosov, and S. I. Simak, *Phys. Rev. B* **84**, 180301(R) (2011).
- <sup>21</sup> O. Hellman, P. Steneteg, I. A. Abrikosov, and S. I. Simak, *Phys. Rev. B* **87**, 104111 (2013).
- <sup>22</sup> O. Hellman and I. A. Abrikosov, *Phys. Rev. B* **88**, 144301 (2013).
- <sup>23</sup> N. Shulumba, O. Hellman, and A. J. Minnich, *Phys. Rev. B* **95**, 014302 (2017).
- <sup>24</sup> X. Gonze, F. Jollet, F. A. Araujo, D. Adams, B. Amadon, T. Applencourt, C. Audouze, J.-M. Beuken, J. Bieder, A. Bokhanchuk, E. Bousquet, F. Bruneval, D. Caliste, M. Côté, F. Dahm, F. D. Pieve, M. Delaveau, M. D. Genaro, B. Dorado, C. Espejo, G. Geneste, L. Genovese, A. Gerossier, M. Giantomassi, Y. Gillet, D. Hamann, L. He, G. Jomard, J. L. Janssen, S. L. Roux, A. Levitt, A. Lherbier, F. Liu, I. Lukačević, A. Martin, C. Martins, M. Oliveira, S. Poncé, Y. Pouillon, T. Rangel, G.-M. Rignanese, A. Romero, B. Rousseau, O. Rubel, A. Shukri, M. Stankovski, M. Torrent, M. V. Setten, B. V. Troeye, M. Verstraete, D. Waroquiers, J. Wiktor, B. Xu, A. Zhou, and J. Zwanziger, *Comput. Phys. Commun.* **205**, 106 (2016).
- <sup>25</sup> X. Gonze, B. Amadon, P.-M. Anglade, J.-M. Beuken, F. Bottin, P. Boulanger, F. Bruneval, D. Caliste, R. Caracas, M. Côté, T. Deutsch, L. Genovese, P. Ghosez, M. Giantomassi, S. Goedecker, D. Hamann, P. Hermet, F. Jollet, G. Jomard, S. Leroux, M. Mancini, S. Mazevet, M. Oliveira, G. Onida, Y. Pouillon, T. Rangel, G.-M. Rignanese, D. Sangalli, R. Shaltaf, M. Torrent, M. Verstraete, G. Zerah, and J. Zwanziger, *Comput. Phys. Commun.* **180**, 2582 (2009), 40 YEARS OF CPC: A celebratory issue focused on quality software for high performance, grid and novel computing architectures.
- <sup>26</sup> J. P. Perdew and A. Zunger, *Phys. Rev. B* **23**, 5048 (1981).
- <sup>27</sup> C. Hartwigsen, S. Goedecker, and J. Hutter, *Phys. Rev. B* **58**, 3641 (1998).
- <sup>28</sup> J. Cao, J. Querales-Flores, S. Fahy, and I. Savić, *Mater. Today Phys.* **12**, 100172 (2020).
- <sup>29</sup> G. Kresse and J. Furthmüller, *Comput. Phys. Commun.* **6**, 15 (1996).
- <sup>30</sup> J. Heyd, G. E. Scuseria, and M. Ernzerhof, *J. Chem. Phys.* **118**, 8207 (2003).
- <sup>31</sup> J. Heyd and G. E. Scuseria, *J. Chem. Phys.* **121**, 1187 (2004).
- <sup>32</sup> G. Kresse and D. Joubert, *Phys. Rev. B* **59**, 1758 (1999).
- <sup>33</sup> J. D. Querales-Flores, J. Cao, S. Fahy, and I. Savić, *Phys. Rev. Mater.* **3**, 055405 (2019).
- <sup>34</sup> P. B. Allen and V. Heine, *J. Phys. C: Solid State* **9**, 2305 (1976).
- <sup>35</sup> P. B. Allen and M. Cardona, *Phys. Rev. B* **23**, 1495 (1981).
- <sup>36</sup> P. B. Allen and M. Cardona, *Phys. Rev. B* **27**, 4760 (1983).
- <sup>37</sup> X. Gonze and C. Lee, *Phys. Rev. B* **55**, 10355 (1997).
- <sup>38</sup> S. Baroni, S. de Gironcoli, A. Dal Corso, and P. Giannozzi, *Rev. Mod. Phys.* **73**, 515 (2001).
- <sup>39</sup> S. Poncé, Y. Gillet, J. L. Janssen, A. Marini, M. Verstraete, and X. Gonze, *J. Chem. Phys.* **143**, 102813 (2015).
- <sup>40</sup> M. S. Dresselhaus, G. Dresselhaus, and A. Jorio, *Group Theory: Application to the Physics of Condensed Matter*, 1st ed. (Springer-Verlag Berlin Heidelberg, 2008) pp. 97, 246, 254–255.
- <sup>41</sup> P. Giannozzi, S. Baroni, N. Bonini, M. Calandra, R. Car, C. Cavazzoni, D. Ceresoli, G. L. Chiarotti, M. Cococcioni, I. Dabo, A. Dal Corso, S. de Gironcoli, S. Fabris, G. Fratesi, R. Gebauer, U. Gerstmann, C. Gougousis, A. Kokalj, M. Lazzeri, L. Martin-Samos, N. Marzari, F. Mauri, R. Mazzarello, S. Paolini, A. Pasquarello, L. Paulatto, C. Sbraccia, S. Scandolo, G. Sclauzero, A. P. Seitsonen, A. Smogunov, P. Umari, and R. M. Wentzcovitch, *J. Phys. Condens. Matter* **21**, 395502 (19pp) (2009).
- <sup>42</sup> P. Giannozzi, O. Andreussi, T. Brumme, O. Bunau, M. B. Nardelli, M. Calandra, R. Car, C. Cavazzoni, D. Ceresoli, M. Cococcioni, N. Colonna, I. Carnimeo, A. D. Corso, S. de Gironcoli, P. Delugas, R. A. D. Jr, A. Ferretti, A. Floris, G. Fratesi, G. Fugallo, R. Gebauer, U. Gerstmann, F. Giustino, T. Gorni, J. Jia, M. Kawamura, H.-Y. Ko, A. Kokalj, E. Küçükbenli, M. Lazzeri, M. Marsili, N. Marzari, F. Mauri, N. L. Nguyen, H.-V. Nguyen, A. O. de-la Roza, L. Paulatto, S. Poncé, D. Rocca, R. Sabatini, B. Santra, M. Schlipf, A. P. Seitsonen, A. Smogunov, I. Timrov, T. Thonhauser, P. Umari, N. Vast, X. Wu, and S. Baroni, *J. Phys. Condens. Matter* **29**, 465901 (2017).
- <sup>43</sup> A. R. Murphy, F. Murphy-Armando, S. Fahy, and I. Savić, *Phys. Rev. B* **98**, 085201 (2018).
- <sup>44</sup> S. Poncé, E. Margine, C. Verdi, and F. Giustino, *Comput. Phys. Commun.* **209**, 116 (2016).
- <sup>45</sup> A. A. Mostofi, J. R. Yates, G. Pizzi, Y.-S. Lee, I. Souza, D. Vanderbilt, and N. Marzari, *Comput. Phys. Commun.* **185**, 2309 (2014).
- <sup>46</sup> F. Murphy-Armando and S. Fahy, *Phys. Rev. B* **78**, 035202 (2008).
- <sup>47</sup> C. Herring and E. Vogt, *Phys. Rev.* **101**, 944 (1956).
- <sup>48</sup> B. K. Ridley, “Quantum processes in semiconductors,” (Oxford University Press, Oxford, UK, 1999) pp. 143–144.
- <sup>49</sup> I. I. Ravich, *Semiconducting lead chalcogenides*, Vol. 5 (Springer Science & Business Media, 2013).
- <sup>50</sup> M. P. Jiang, M. Trigo, I. Savić, S. Fahy, É. D. Murray, C. Bray, J. Clark, T. Henighan, M. Kozina, M. Chollet, J. M. Glowia, M. C. Hoffmann, D. Zhu, O. Delaire, A. F. May, B. C. Sales, A. M. Lindenberg, P. Zalden, T. Sato, R. Merlin, and D. A. Reis, *Nat. Commun.* **7**, 12291 (2016).
- <sup>51</sup> M. S. Dresselhaus, G. Dresselhaus, and A. Jorio, *Group Theory: Application to the Physics of Condensed Matter*, 1st ed. (Springer-Verlag Berlin Heidelberg, 2008).
- <sup>52</sup> G. A. S. Ribeiro, L. Paulatto, R. Bianco, I. Errea, F. Mauri, and M. Calandra, *Phys. Rev. B* **97**, 014306 (2018).
- <sup>53</sup> P. Chudzinski, *Phys. Rev. Research* **2**, 012048(R) (2020).